THE ASTRONOMICAL JOURNAL VOLUME 112, NUMBER 3 SEPTEMBER 1996

THE MAUNA KEA–CERRO-TOLOLO (MKCT) KUIPER BELT AND CENTAUR SURVEY

DAVID JEWITT[1]
Institute for Astronomy, 2680 Woodlawn Drive, Honolulu, Hawaii 96822
Electronic mail: jewitt@ifa.hawaii.edu

JANE LUU[1]
Astronomy Department, Harvard University, 60 Garden Street, Cambridge, Massachusetts 02138
Electronic mail: luu@cfa.harvard.edu

JUN CHEN
Institute for Astronomy, 2680 Woodlawn Drive, Honolulu, Hawaii 96822
Electronic mail: jchen@ifa.hawaii.edu

Received 1996 April 4; revised 1996 June 7

ABSTRACT

We present the results of a medium depth ecliptic sky survey conducted with telescopes at the Mauna Kea and Cerro-Tololo Observatories. The survey revealed 15 new Kuiper Belt objects, and 2 Centaurs (objects orbiting in the vicinity of the gas giant planets), bringing the total number of Kuiper Belt objects to 32 and Centaurs to 6. We use the new objects to begin to constrain some of the properties of the Kuiper Belt and Centaur populations. The apparent width of the Kuiper Belt is 10° full width at half maximum (FWHM) but, after correcting for the effects of observational selection, we find that the intrinsic width must be at least 30° FWHM. The inferred number of objects in the 30–50 AU heliocentric distance range is 7×10^4 (diameters $\geqslant$100 km). Of these, about 40% ($\approx3\times10^4$) are in or near the 3:2 mean-motion resonance with Neptune. Pluto, which also occupies this resonance, is now seen as the largest of a hitherto unknown family of dynamically similar, resonantly trapped objects. We find that the Centaurs have a sky-plane surface density that is ≈0.5 deg^{-2} to $m_R=24.2$. The total population with absolute magnitude $H_R\leqslant9.5$ (diameter approximately $\geqslant$75 km if albedo ≈0.04) is $N\approx2600$, about an order of magnitude greater than the corresponding number of large main-belt asteroids. We crudely estimate that 1.5 $M_{\rm Earth}$ of material has been cycled from the Kuiper Belt through the Centaurs in the age of the solar system. © *1996 American Astronomical Society.*

1. INTRODUCTION

Starting with 1992 QB_1 (Jewitt & Luu 1993), we have uncovered a substantial population of solar system bodies in orbit beyond Neptune (Jewitt & Luu 1995; hereafter referred to as Paper 1). Additional members of this population have been reported by Irwin *et al.* (1995), Williams *et al.* (1995), and others (see Luu 1994 and Paper 1 for observational reviews). At the time of writing, 32 Kuiper Belt objects have been found (an updated list may be found at http://www.ifa.hawaii.edu/faculty/jewitt/kb.html). There is growing consensus that these bodies are representatives of a trans-Neptunian ring or belt, the existence of which was first postulated by Edgeworth (1949) and Kuiper (1951). This so-called "Kuiper Belt" is a likely product of the pre-planetary accretional phases of the solar system, and may contain the most primitive material accessible to direct investigation. The new observational work has spawned a variety of exciting investigations into the dynamics of the outer solar system (e.g., Holman & Wisdom 1993; Malhotra 1993, 1995, 1996; Duncan *et al.* 1995; Morbidelli *et al.* 1995), with ramifications for the origin of comets (Fernandez 1980; Duncan *et al.* 1988) and the accretion of planetesimals and planets (Bailey 1994).

The discovery of the Kuiper Belt is only the first step in a long journey towards an understanding of the contents, evolution and scientific significance of the outer planetary system. Observationally, there is an acute need to assess the number–magnitude relation for these distant small bodies, using carefully conducted and photometrically well-characterized ecliptic sky surveys. To date, the only such surveys in the literature are our own Paper 1 (7 objects found in 1.2 deg^2 to red magnitude $m_R=24.8$) and Irwin *et al.* (1995) (2 objects found in 0.7 deg^2 to $m_R=23.5$). In the present paper, we discuss results from the Mauna Kea–Cerro-Tololo (MKCT) medium-depth survey that complement our previously published work in area surveyed and limiting magnitude. We use the new observations to constrain not only the Kuiper Belt, but also closer objects in the dynamically distinct family of gas-giant planet crossers or "Centaurs."

[1]Visiting astronomer at the Cerro Tololo Inter-American Observatory, which is operated by the National Optical Astronomy Observatory under contract to the National Science Foundation.

 0004-6256/96/112(3)/1225/14/$10.00

TABLE 1. Instrumental parameters.

Telescope	UH 2.2m	CTIO 1.5m
Focal Ratio	f/10	f/7.5
Detector	Tektronix 2048x2048	Tektronix 2048x2048
Quantum Efficiency	0.9 (coated)	0.45
Image Scale [arcsec/pixel]	0.219 ± 0.001	0.433
Field Area [sq. deg]	0.016	0.061
Read Time [seconds]	100	50

2. OBSERVATIONS

Survey observations were made with both the University of Hawaii (UH) 2.2 m telescope on Mauna Kea and the Cerro-Tololo InterAmerican Observatory (CTIO) 1.5 m telescope. Observations at the UH 2.2 m telescope were taken with a 2048×2048 pixel Tektronix charge-coupled device (CCD). Basic instrumental parameters are summarized in Table 1. Note the extraordinary quantum efficiency of the CCD, obtained by antireflection coating the device. This telescope and detector were the same as used in our previous ecliptic survey work (Jewitt & Luu 1993; Paper 1), with two small but important differences. First, the CCD readout time was reduced to 100 s, making short integrations more observationally efficient. Second, improvements in the autoguider allowed us to reposition the telescope during the readout period, further reducing the dead time between exposures. We elected to use a 300 s integration as standard, and obtained a duty cycle of 75%.

An additional change was the use of a custom made 100-mm-diam broadband filter, designated "*VR*." The *VR* filter transmission is shown in Fig. 1. The filter provides an approximately factor of 2 increase in throughput over the previously used *R* filter, with only a small increase in the sky background (the dominant OH sky lines at $\lambda \geq 7000$ Å are excluded).

Observations at the CTIO 1.5 m were taken with an uncoated Tektronix CCD (the lack of an antireflection coating is the cause of the lower CTIO quantum efficiency reported in Table 1). To partially compensate for the lesser aperture, narrower bandpass, and reduced CCD quantum efficiency, we employed an integration time of 900 s as standard.

At both telescopes, observations were confined to moonless nights judged to be photometric and with good seeing. Where possible, we selected fields along the ecliptic so as to maximize the number of detected objects. We further observed near opposition, where the rate of angular motion across the sky is largely parallactic, and can be simply related to the heliocentric distance (Luu & Jewitt 1988). Observations at opposition also benefit from minimal phase darkening (Bowell *et al.* 1989). Photometric calibration of the data was obtained from observations of standard stars from Landolt 1992.

Three identical images of each field were recorded, with a temporal separation between images of about 1 hr. Since the expected rate of motion of the trans-Neptunians and Centaurs is $\geq 2''$/hr, this timebase is sufficient to detect moving objects. The images were reduced (bias subtracted and flat-fielded) at the telescope, and examined by blinking on a SparcStation at the summit, as well as later, at sea level.

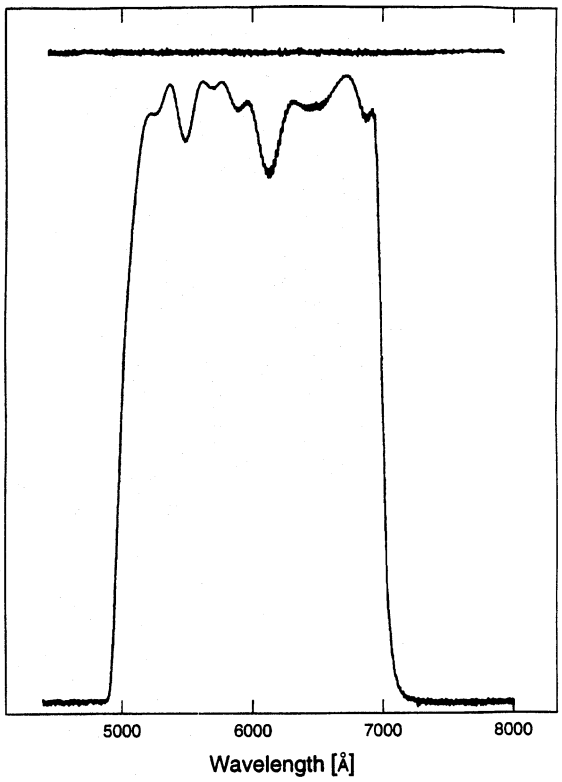

FIG. 1. Transmission of the VR filter as a function of wavelength (Å). The upper horizontal trace marks 100% transmission. 0% transmission falls at the base of the profile.

The effective limiting magnitudes of the images were determined by adding artificial objects to the real data frames and then finding them by the same procedures used to locate trans-Neptunians. By this procedure, we found limiting magnitudes for point sources in the MKO and CTIO data of $m_R = 24.2$ and $m_R = 23.2$, respectively. The quoted magnitudes refer to a detection probability of 50%. Measured in the same way, our previous MKO survey had limiting magnitude $m_R = 24.8$ (Paper 1).

The effective limiting magnitude is poorer for moving objects than for stationary ones as a result of spreading the light. The "trailing loss," Δm_R (magnitude), is estimated from

$$\Delta m_R = 0 \quad \psi \leq 1,$$
$$\Delta m_R = 2.5 \log(\psi) \quad \psi > 1, \tag{1}$$

where $\psi = \dot{\theta} t / \theta_{\rm FWHM}$, and $\dot{\theta}$ (arcsec/hr) is the opposition proper motion, t (hr) is the integration time, and $\theta_{\rm FWHM}$ (arcsec) is the seeing. Equation (1) is plotted for the MKO data ($t = 0.083$ hr, $\theta_{\rm FWHM} = 0.8$ arcsec) and CTIO data ($t = 0.25$ hr, $\theta_{\rm FWHM} = 1.0$ arcsec) in Fig. 2. The figure shows that trailing loss is negligible for the slowly moving trans-Neptunian objects in both the MKO 5 min and CTIO 15 min data. The high angular rates of Centaurs, however, cause substantial trailing loss in the long exposures of the CTIO data, and even in the short exposure MKO data at distances inside the orbit of Saturn. Accordingly, we use the MKO data to pro-

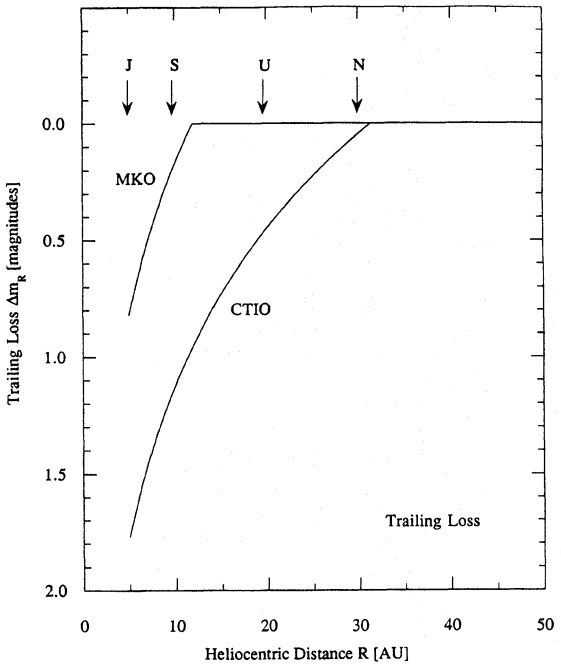

FIG. 2. Trailing loss as a function of heliocentric distance, computed from Eq. (1). The marked curves refer to the Mauna Kea and Cerro-Tololo observations. Heliocentric distances of the major planets are marked.

vide constraints on the Kuiper Belt and on the Centaur population at heliocentric distances $R \geq 10$ AU, but use the Cerro-Tololo data only for objects in the Kuiper Belt ($R \geq 30$ AU).

3. RESULTS

The coordinates of the survey fields are listed in Tables 2 (MKO) and 3 (CTIO). At MKO, we surveyed 3.9 deg^2 to $m_R = 24.2$, and discovered 12 Kuiper Belt objects and 2 Centaurs. In the CTIO data, the corresponding numbers are 4.4 deg^2, $m_R = 23.2$, for 3 Kuiper Belt objects and 0 Centaurs (consistent with the expected large trailing loss as discussed above). Parameters of the 17 newly discovered objects are given in Table 4. For each object, we present the heliocentric and geocentric distances, and phase angle, at the date of discovery. The apparent red magnitude at discovery is also listed, together with the absolute magnitude, H_R, on the Bowell–Lumme (Bowell *et al.* 1989) system. To correct apparent magnitudes, m_R, to H_R we assumed $G = 0.15$, as is appropriate for dark asteroids observed in the inner solar system. Notice that m_R and H_R refer to instantaneous measurements of the brightness of each object, and ignore the possible effects of rotational modulation of the cross section (e.g., Williams *et al.* 1995). More complete multiwavelength photometry of these and other slow moving objects is discussed in a parallel paper (Luu & Jewitt 1996). In Table 4 we also list the diameter, D (km), calculated from H_R assuming a geometric albedo $p_R = 0.04$. This is comparable to the albedos of the nuclei of short period comets (cf. Table II of Jewitt 1996). Diameters for other adopted values of p_R may be calculated from Table 4 using $p_R D^2 = \text{constant}$.

The orbital elements of the newly discovered objects are given in Table 5. These elements were computed by Brian Marsden (Smithsonian Center for Astrophysics) and published by him in the Minor Planet Electronic Circulars (MPECs). Elements of the 17 objects which have been observed at more than one opposition are, for the most part, relatively secure. In some other cases, insufficient astrometry exists, and a circular orbit ($e = 0$) has been assumed. The table is preliminary, in the sense that the orbital elements will be refined as new astrometry becomes available, but the gross properties are expected to remain unchanged.

The cumulative, sky-plane surface densities of the Kuiper Belt objects are summarized in Table 6. The uncertainties in this table are 1σ errors computed by assuming Poisson statistics and noting where the surface density drops to $1/e$ of the measured value. Also listed in Table 6 are surface densities obtained from other surveys, as noted. Where comparisons are possible (notably between the results of MKCT, Paper 1 and Irwin *et al.* 1995), the agreement is generally rather good. In fact, the differences between surface densities derived from different surveys provide a more direct and therefore compelling estimate of the experimental repeatability of the measurements than do the Poisson error bars.

With the enlarged data sample (Table 6), the slope of the magnitude-frequency plot for the Kuiper Belt (Fig. 3) is better defined than previously. In the range $23.2 \leq m_R \leq 24.8$, the surface density of objects varies as $\log \Sigma_{TN} = -8(\pm 3) + 0.4(\pm 0.1)\, m_R$, corresponding to an increase in the cumulative surface density by a factor of 2.5 per magnitude. As discussed in Paper 1, the slope is a measure of the size distribution of the Kuiper Belt objects, but one that is convolved with the radial density distribution and with the magnitude limit of the survey itself. Figure 3 shows a Monte Carlo model for a magnitude limited survey in which we represent the radial density distribution by a power law having index $p = 2$. The differential size distribution is assumed to obey

$$n(a)da = \Gamma a^{-q} da, \tag{2}$$

with Γ=constant and $q = 3$. The size distribution extends to a maximum radius $a_+ = 1000$ km (upper curve) and $a_+ = 250$ km (lower curve). For $m_R \geq 22$, the models are insensitive to a_+, and the slope of the magnitude-frequency plot is faithfully reproduced. Substantially shallower (e.g., $q = 2$) or steeper (e.g., $q = 4$) size distributions violate the data in Fig. 3, and we thus conclude that the size distribution of the 100–400 km diameter objects is close to inverse cube. Interestingly, this slope is close to that inferred for the size distribution of cometary nuclei (Shoemaker & Wolfe 1982). We also note that a line fitted to the $23.2 \leq m_R \leq 24.8$ Kuiper Belt objects passes neatly though Tombaugh's (1961) datum (point T). For $17 < m_R < 22$, the observational situation is less clear. The upper limits from the Schmidt surveys of Luu & Jewitt (1988) [point LJ (S)] and, especially, Kowal (1989) (point K) violate any simple interpolation. While we have no specific reason to doubt these surveys, we nevertheless believe that it would be extremely worthwhile to repeat them using modern, digital detectors.

Also in Fig. 3 we have plotted Cochran *et al.*'s (1995) reported statistical detection of ultra-faint Kuiper Belt ob-

TABLE 2. Observations from the University of Hawaii 2.2 m Telescope on Mauna Kea, Hawaii.

Field	UT Date	Tel	RA(2000)	Dec(2000)	Filter	Integration	Objects Detected
T16a	94/Sep/29	UH88	21:12:50	02:40:00	VR	300x3	
T16b	94/Sep/29	UH88	21:13:20	02:40:02	VR	300x3	
T16c	94/Sep/29	UH88	21:13:50	02:40:03	VR	300x3	
T16d	94/Sep/29	UH88	21:14:20	02:40:05	VR	300x3	
T16e	94/Sep/29	UH88	21:14:50	02:40:06	VR	300x3	
T38a	94/Sep/29	UH88	22:59:39	02:40:00	VR	300x3	
T38b	94/Sep/29	UH88	23:00:09	02:40:02	VR	300x3	
T38c	94/Sep/29	UH88	23:00:39	02:40:04	VR	300x3	
T38d	94/Sep/29	UH88	23:01:10	02:40:06	VR	300x3	
T38e	94/Sep/29	UH88	23:01:39	02:40:07	VR	300x3	
T41a	94/Oct/02	UH88	23:14:13	02:40:00	VR	300x3	1994 TB (MPEC1994.T02)
T41b	94/Oct/02	UH88	23:14:44	02:40:00	VR	300x3	
T41c	94/Oct/02	UH88	23:15:14	02:40:00	VR	300x3	
T41d	94/Oct/02	UH88	23:15:44	02:40:00	VR	300x3	
T41e	94/Oct/02	UH88	23:16:14	02:40:00	VR	300x3	
T48a	94/Oct/02	UH88	23:48:13	02:40:00	VR	300x3	
T48b	94/Oct/02	UH88	23:48:43	02:40:00	VR	300x3	
T48c	94/Oct/02	UH88	23:49:13	02:40:00	VR	300x3	
T48d	94/Oct/02	UH88	23:49:43	02:40:00	VR	300x3	
T48e	94/Oct/02	UH88	23:50:13	02:40:00	VR	300x3	
T66a	94/Oct/02	UH88	01:15:37	02:40:00	VR	300x3	
T66b	94/Oct/02	UH88	01:16:07	02:40:00	VR	300x3	1994 TA (MPEC1994.T01)
T66c	94/Oct/02	UH88	01:16:37	02:40:00	VR	300x3	
T66d	94/Oct/02	UH88	01:17:07	02:40:00	VR	300x3	
T66e	94/Oct/02	UH88	01:17:37	02:40:00	VR	300x3	
T36a	94/Oct/03	UH88	22:49:57	02:40:00	VR	300x3	
T36b	94/Oct/03	UH88	22:50:27	02:40:00	VR	300x3	
T36c	94/Oct/03	UH88	22:50:57	02:40:00	VR	300x3	
T36d	94/Oct/03	UH88	22:51:27	02:40:00	VR	300x3	
T36e	94/Oct/03	UH88	22:51:57	02:40:00	VR	300x3	
T44a	94/Oct/03	UH88	23:28:47	02:40:00	VR	300x3	
T44b	94/Oct/03	UH88	23:29:17	02:40:00	VR	300x3	
T44c	94/Oct/03	UH88	23:29:47	02:40:00	VR	300x3	
T44d	94/Oct/03	UH88	23:30:17	02:40:00	VR	300x3	
T44e	94/Oct/03	UH88	23:30:47	02:40:00	VR	300x3	
T57a	94/Oct/03	UH88	00:31:55	02:40:00	VR	300x3	
T57b	94/Oct/03	UH88	00:32:25	02:40:00	VR	300x3	
T57c	94/Oct/03	UH88	00:32:55	02:40:00	VR	300x3	1994 TG ((MPEC 1994.T03)
T57d	94/Oct/03	UH88	00:33:25	02:40:00	VR	300x3	
T57e	94/Oct/03	UH88	00:33:55	02:40:00	VR	300x3	1994 TH (MPEC1994.T04)
ECL768	95/Feb/24	UH88	08:33:16	18:47:15	VR	300x3	
ECL769	95/Feb/24	UH88	08:35:20	18:39:43	VR	300x3	1995 DA2 (MPEC1995.E05)
ECL770	95/Feb/24	UH88	08:37:25	18:32:04	VR	300x3	
ECL771	95/Feb/24	UH88	08:39:29	18:24:21	VR	300x3	1995 DB2 (MPEC1995.E06)
ECL772	95/Feb/24	UH88	08:41:34	18:16:31	VR	300x3	
ECL773	95/Feb/24	UH88	08:43:38	18:08:37	VR	300x3	
ECL774	95/Feb/24	UH88	08:45:41	18:00:39	VR	300x3	
ECL816	95/Feb/24	UH88	10:09:18	11:23:11	VR	300x3	
ECL817	95/Feb/24	UH88	10:11:13	11:12:31	VR	300x3	
ECL818	95/Feb/24	UH88	10:13:08	11:01:48	VR	300x3	
ECL819	95/Feb/24	UH88	10:15:04	10:57:01	VR	300x3	
ECL820	95/Feb/24	UH88	10:16:59	10:40:14	VR	300x3	1995 DC2 (MPEC1995.E07)
ECL821	95/Feb/24	UH88	10:18:53	10:29:24	VR	300x3	
ECL822	95/Feb/24	UH88	10:20:48	10:18:30	VR	300x3	
ECL775	95/Feb/25	UH88	08:47:45	17:52:35	VR	300x3	
ECL776	95/Feb/25	UH88	08:49:48	17:44:25	VR	300x3	
ECL777	95/Feb/25	UH88	08:51:52	17:36:13	VR	300x3	
ECL778	95/Feb/25	UH88	08:53:55	17:27:55	VR	300x3	
ECL779	95/Feb/25	UH88	08:55:57	17:19:32	VR	300x3	
ECL780	95/Feb/25	UH88	08:58:00	17:11:04	VR	300x3	
ECL781	95/Feb/25	UH88	09:00:02	17:02:32	VR	300x3	
ECL782	95/Feb/25	UH88	09:02:04	16:53:57	VR	300x3	
ECL881	95/Feb/25	UH88	12:10:06	-01:05:38	VR	300x3	

TABLE 2. (continued)

Field	UT Date	Tel	RA(2000)	Dec(2000)	Filter	Integration	Objects Detected
ECL783	95/Feb/26	UH88	09:04:06	16:45:19	VR	300x3	
ECL784	95/Feb/26	UH88	09:06:08	16:36:31	VR	300x3	
ECL785	95/Feb/26	UH88	09:08:10	16:27:42	VR	300x3	
ECL786	95/Feb/26	UH88	09:10:11	16:18:48	VR	300x3	
ECL787	95/Feb/26	UH88	09:12:12	16:09:50	VR	300x3	
ECL788	95/Feb/26	UH88	09:14:13	16:00:49	VR	300x3	
ECL789	95/Feb/26	UH88	09:16:13	15:51:42	VR	300x3	
ECL843	95/Feb/26	UH88	11:00:22	06:21:57	VR	300x3	
ECL844	95/Feb/26	UH88	11:02:14	06:10:23	VR	300x3	
ECL845	95/Feb/26	UH88	11:04:05	05:58:47	VR	300x3	
ECL846	95/Feb/26	UH88	11:05:56	05:47:11	VR	300x3	
ECL847	95/Feb/26	UH88	11:07:48	05:35:33	VR	300x3	
ECL848	95/Feb/26	UH88	11:09:39	05:23:56	VR	300x3	
ECL849	95/Feb/26	UH88	11:11:30	05:12:15	VR	300x3	
ECL768a	95/Feb/27	UH88	08:33:16	18:55:16	VR	300x3	
ECL768b	95/Feb/27	UH88	08:33:16	19:03:17	VR	300x3	
ECL768c	95/Feb/27	UH88	08:33:16	19:11:17	VR	300x3	
ECL768d	95/Feb/27	UH88	08:33:16	18:39:16	VR	300x3	
ECL768e	95/Feb/27	UH88	08:33:16	18:31:17	VR	300x3	
ECL768f	95/Feb/27	UH88	08:33:16	18:23:17	VR	300x3	
ECL768g	95/Feb/27	UH88	08:33:16	18:15:17	VR	300x3	
ECL884a	95/Feb/27	UH88	12:15:34	-01:33:08	VR	300x3	
ECL884b	95/Feb/27	UH88	12:15:34	-01:25:05	VR	300x3	
ECL884c	95/Feb/27	UH88	12:15:34	-01:17:01	VR	300x3	1995 DW2 (MPEC1995.E13)
ECL884d	95/Feb/27	UH88	12:15:34	-01:09:01	VR	300x3	
ECL884e	95/Feb/27	UH88	12:15:34	-01:49:02	VR	300x3	
ECL884f	95/Feb/27	UH88	12:15:34	-01:56:57	VR	300x3	
ECL884g	95/Feb/27	UH88	12:15:34	-02:05:01	VR	300x3	
ECL1020a	95/Apr/03	UH88	10:37:53	08:38:52	VR	300x3	
ECL1020b	95/Apr/03	UH88	10:37:20	08:38:55	VR	300x3	1995 GJ (MPEC1995.G07)
ECL1020c	95/Apr/03	UH88	10:36:48	08:38:58	VR	300x3	
ECL1020d	95/Apr/03	UH88	10:36:48	08:46:57	VR	300x3	
ECL1020e	95/Apr/03	UH88	10:37:20	08:46:57	VR	300x3	
ECL1020f	95/Apr/03	UH88	10:37:52	08:46:55	VR	300x3	
ECL1100a	95/Apr/03	UH88	13:04:46	-06:48:36	VR	300x3	
ECL1100b	95/Apr/03	UH88	13:04:14	-06:48:38	VR	300x3	
ECL1100c	95/Apr/03	UH88	13:03:43	-06:48:40	VR	300x3	
ECL1100d	95/Apr/03	UH88	13:03:43	-06:40:36	VR	300x3	
ECL1100e	95/Apr/03	UH88	13:04:15	-06:40:37	VR	300x3	
ECL1100f	95/Apr/03	UH88	13:04:46	-06:40:36	VR	300x3	1995 GA7 (MPEC.G13)
ECL1138a	95/Apr/03	UH88	14:15:17	-13:33:58	VR	300x3	
ECL1138b	95/Apr/03	UH88	14:14:44	-13:33:54	VR	300x3	
ECL1138c	95/Apr/03	UH88	14:14:11	-13:33:52	VR	300x3	
ECL1138d	95/Apr/03	UH88	14:14:10	-13:25:51	VR	300x3	
ECL1138e	95/Apr/03	UH88	14:14:44	-13:25:52	VR	300x3	
ECL1138f	95/Apr/03	UH88	14:15:17	-13:25:54	VR	300x3	
ECL1040a	95/Apr/04	UH88	11:15:12	04:48:56	VR	300x3	
ECL1040b	95/Apr/04	UH88	11:14:40	04:49:01	VR	300x3	
ECL1040c	95/Apr/04	UH88	11:14:08	04:49:04	VR	300x3	
ECL1040d	95/Apr/04	UH88	11:14:08	04:57:05	VR	300x3	
ECL1040e	95/Apr/04	UH88	11:14:40	04:57:04	VR	300x3	
ECL1040f	95/Apr/04	UH88	11:15:12	04:49:03	VR	300x3	
ECL1116a	95/Apr/04	UH88	13:34:31	-09:49:27	VR	300x3	
ECL1116b	95/Apr/04	UH88	13:33:59	-09:49:23	VR	300x3	
ECL1116c	95/Apr/04	UH88	13:33:26	-09:49:20	VR	300x3	
ECL1116d	95/Apr/04	UH88	13:33:26	-09:41:20	VR	300x3	
ECL1116e	95/Apr/04	UH88	13:33:59	-09:41:28	VR	300x3	
ECL1116f	95/Apr/04	UH88	13:34:31	-09:41:29	VR	300x3	
ECL1146a	95/Apr/04	UH88	14:30:07	-14:59:19	VR	300x3	
ECL1146b	95/Apr/04	UH88	14:29:34	-14:59:17	VR	300x3	
ECL1146c	95/Apr/04	UH88	14:29:01	-14:59:15	VR	300x3	
ECL1146d	95/Apr/04	UH88	14:29:01	-14:51:15	VR	300x3	
ECL1146e	95/Apr/04	UH88	14:29:34	-14:51:15	VR	300x3	
ECL1146f	95/Apr/04	UH88	14:30:07	-14:51:17	VR	300x3	

TABLE 2. (continued)

Field	UT Date	Tel	RA(2000)	Dec(2000)	Filter	Integration	Objects Detected
ECL1124a	95/Apr/05	UH88	13:49:02	-11:13:47	VR	300x3	
ECL1124b	95/Apr/05	UH88	13:48:29	-11:13:41	VR	300x3	
ECL1124c	95/Apr/05	UH88	13:47:56	-11:13:55	VR	300x3	
ECL1124d	95/Apr/05	UH88	13:47:56	-11:05:35	VR	300x3	
ECL1124e	95/Apr/05	UH88	13:48:29	-11:05:35	VR	300x3	
ECL1124f	95/Apr/05	UH88	13:49:01	-11:05:35	VR	300x3	
ECL1144a	95/Apr/05	UH88	14:26:39	-14:30:50	VR	300x3	
ECL1144b	95/Apr/05	UH88	14:26:06	-14:30:48	VR	300x3	
ECL1144c	95/Apr/05	UH88	14:25:33	-14:30:45	VR	300x3	
ECL1144d	95/Apr/05	UH88	14:25:34	-14:22:45	VR	300x3	
ECL1144e	95/Apr/05	UH88	14:26:06	-14:22:45	VR	300x3	
ECL1144f	95/Apr/05	UH88	14:26:39	-14:22:47	VR	300x3	
ECL1032a	95/Apr/05	UH88	11:00:22	06:21:57	VR	300x3	
ECL1032b	95/Apr/05	UH88	10:59:50	06:22:04	VR	300x3	
ECL1032c	95/Apr/05	UH88	10:59:17	06:22:09	VR	300x3	
ECL1032d	95/Apr/05	UH88	10:59:17	06:30:10	VR	300x3	
ECL1032e	95/Apr/05	UH88	10:59:50	06:30:10	VR	300x3	
ECL1032f	95/Apr/05	UH88	11:00:22	06:30:10	VR	300x3	
ECL1098a	95/Apr/06	UH88	13:01:07	-06:31:01	VR	300x3	
ECL1098b	95/Apr/06	UH88	13:00:34	-06:30:59	VR	300x3	
ECL1098c	95/Apr/06	UH88	13:00:02	-06:30:57	VR	300x3	
ECL1098d	95/Apr/06	UH88	13:00:02	-06:22:57	VR	300x3	
ECL1098e	95/Apr/06	UH88	13:00:34	-06:22:59	VR	300x3	
ECL1098f	95/Apr/06	UH88	13:01:07	-06:23:00	VR	300x3	
T150a	95/May/30	UH88	15:00:30	-17:11:01	VR	300x3	
T150b	95/May/30	UH88	15:01:03	-17:11:01	VR	300x3	
T150c	95/May/30	UH88	15:01:37	-17:11:03	VR	300x3	1995 KJ1 (MPEC 1995.L03)
T150d	95/May/30	UH88	15:01:37	-17:03:03	VR	300x3	1995 KK1 (MPEC 1995.L04)
T150e	95/May/30	UH88	15:01:03	-17:03:00	VR	300x3	
T150f	95/May/30	UH88	15:00:30	-17:02:58	VR	300x3	
T196a	95/May/30	UH88	16:26:46	-21:50:33	VR	300x3	
T196b	95/May/30	UH88	16:27:21	-21:50:32	VR	300x3	
T196c	95/May/30	UH88	16:27:55	-21:50:33	VR	300x3	
T196d	95/May/30	UH88	16:26:46	-21:42:22	VR	300x3	
T196e	95/May/30	UH88	16:27:21	-21:42:23	VR	300x3	
T196f	95/May/30	UH88	16:26:46	-21:42:28	VR	300x3	
T205a	95/May/31	UH88	16:44:20	-22:18:50	VR	300x3	
T205b	95/May/31	UH88	16:43:45	-22:18:47	VR	300x3	
T205c	95/May/31	UH88	16:43:11	-22:18:45	VR	300x3	
T205d	95/May/31	UH88	16:43:11	-22:26:45	VR	300x3	
T205e	95/May/31	UH88	16:43:45	-22:26:46	VR	300x3	
T205f	95/May/31	UH88	16:44:20	-22:26:47	VR	300x3	
T272a	95/May/31	UH88	18:57:33	-10:45:53	VR	300x3	
T272b	95/May/31	UH88	18:57:00	-10:45:51	VR	300x3	
T272c	95/May/31	UH88	18:57:00	-10:53:51	VR	300x3	
T272d	95/May/31	UH88	18:57:33	-10:53:52	VR	300x3	
T272e	95/May/31	UH88	18:58:05	-10:53:54	VR	300x3	
T272f	95/May/31	UH88	18:58:05	-10:45:53	VR	300x3	
T305a	95/Aug/28	UH88	20:19:35	-19:34:23	VR	300x3	
T305b	95/Aug/28	UH88	20:20:07	-19:34:23	VR	300x3	
T305c	95/Aug/28	UH88	20:20:39	-19:34:23	VR	300x3	
T305d	95/Aug/28	UH88	20:20:39	-19:26:54	VR	300x3	
T305e	95/Aug/28	UH88	20:20:07	-19:26:53	VR	300x3	
T305f	95/Aug/28	UH88	20:19:36	-19:26:53	VR	300x3	
T336a	95/Aug/28	UH88	22:11:46	-11:09:24	VR	300x3	
T336b	95/Aug/28	UH88	22:12:16	-11:09:25	VR	300x3	
T336c	95/Aug/28	UH88	22:12:47	-11:09:25	VR	300x3	
T336d	95/Aug/28	UH88	22:12:47	-11:01:57	VR	300x3	
T336e	95/Aug/28	UH88	22:12:16	-11:01:56	VR	300x3	
T336f	95/Aug/28	UH88	22:11:46	-11:01:55	VR	300x3	
T376a	95/Aug/28	UH88	00:25:13	02:43:30	VR	300x3	
T376b	95/Aug/28	UH88	00:25:43	02:43:29	VR	300x3	
T376c	95/Aug/28	UH88	00:26:13	02:43:28	VR	300x3	
T376d	95/Aug/28	UH88	00:26:13	02:50:58	VR	300x3	
T376e	95/Aug/28	UH88	00:25:43	02:50:59	VR	300x3	
T376f	95/Aug/28	UH88	00:25:13	02:51:00	VR	300x3	

TABLE 2. (continued)

Field	UT Date	Tel	RA(2000)	Dec(2000)	Filter	Integration	Objects Detected
T323a	95/Aug/29	UH88	21:25:59	-15:06:15	VR	300x3	
T323b	95/Aug/29	UH88	21:26:30	-15:06:15	VR	300x3	
T323c	95/Aug/29	UH88	21:27:01	-15:06:15	VR	300x3	
T323d	95/Aug/29	UH88	21:27:01	-14:58:46	VR	300x3	
T323e	95/Aug/29	UH88	21:26:30	-14:58:46	VR	300x3	
T323f	95/Aug/29	UH88	21:25:59	-14:58:44	VR	300x3	
T344a	95/Aug/29	UH88	22:39:10	-08:31:00	VR	300x3	
T344b	95/Aug/29	UH88	22:39:40	-08:31:01	VR	300x3	
T344c	95/Aug/29	UH88	22:40:11	-08:31:01	VR	300x3	
T344d	95/Aug/29	UH88	22:39:11	-08:23:31	VR	300x3	
T344e	95/Aug/29	UH88	22:39:40	-08:23:30	VR	300x3	
T344f	95/Aug/29	UH88	22:39:10	-08:23:29	VR	300x3	
TGA	95/Aug/29	UH88	00:37:22	03:16:25	VR	400x3	
TGB	95/Aug/29	UH88	00:37:52	03:16:24	VR	400x3	
TGC	95/Aug/29	UH88	00:38:22	03:16:22	VR	400x3	
TGD	95/Aug/29	UH88	00:38:22	03:23:51	VR	400x3	
TGE	95/Aug/29	UH88	00:37:52	03:23:52	VR	400x3	1995 QZ9 (MPEC 1995.W11)
TGF	95/Aug/29	UH88	00:37:22	03:23:53	VR	400x3	
T324a	95/Aug/30	UH88	21:29:34	-14:49:08	VR	300x3	
T324b	95/Aug/30	UH88	21:30:05	-14:49:08	VR	300x3	
T324c	95/Aug/30	UH88	21:30:36	-14:49:08	VR	300x3	
T324d	95/Aug/30	UH88	21:30:38	-14:41:39	VR	300x3	
T324e	95/Aug/30	UH88	21:30:05	-14:41:37	VR	300x3	
T324f	95/Aug/30	UH88	21:29:34	-14:14:38	VR	300x3	
T350a	95/Aug/30	UH88	22:59:25	-06:27:45	VR	300x3	
T350b	95/Aug/30	UH88	22:59:55	-06:27:46	VR	300x3	
T350c	95/Aug/30	UH88	23:00:25	-06:27:47	VR	300x3	
T350d	95/Aug/30	UH88	23:00:24	-06:27:17	VR	300x3	
T350e	95/Aug/30	UH88	22:59:55	-06:27:16	VR	300x3	
T350f	95/Aug/30	UH88	22:59:25	-06:27:16	VR	300x3	
T316a	95/Aug/31	UH88	21:00:35	-17:00:05	VR	300x3	
T316b	95/Aug/31	UH88	21:01:07	-17:00:05	VR	300x3	
T316c	95/Aug/31	UH88	21:01:32	-17:00:05	VR	300x3	
T316d	95/Aug/31	UH88	21:01:38	-16:52:36	VR	300x3	
T316e	95/Aug/31	UH88	21:01:07	-16:52:33	VR	300x3	
T316f	95/Aug/31	UH88	21:00:35	-16:52:34	VR	300x3	
T346a	95/Aug/31	UH88	22:45:57	-07:50:17	VR	300x3	
T346b	95/Aug/31	UH88	22:46:27	-07:50:18	VR	300x3	
T346c	95/Aug/31	UH88	22:46:57	-07:50:19	VR	300x3	
T346d	95/Aug/31	UH88	22:46:57	-07:42:43	VR	300x3	
T346e	95/Aug/31	UH88	22:46:27	-07:42:47	VR	300x3	
T346f	95/Aug/31	UH88	22:45:56	-07:42:47	VR	300x3	
TGA	95/Aug/31	UH88	00:37:22	03:16:25	VR	300x3	1995 QY9 (MPEC 1995.W01)
T375a	95/Aug/31	UH88	00:21:56	02:22:20	VR	300x3	
T375b	95/Aug/31	UH88	00:22:26	02:22:20	VR	300x3	
T375c	95/Aug/31	UH88	00:22:56	02:22:19	VR	300x3	
T375d	95/Aug/31	UH88	00:22:56	02:29:47	VR	300x3	
T375e	95/Aug/31	UH88	00:22:26	02:29:48	VR	300x3	
T375f	95/Aug/31	UH88	00:21:56	02:29:49	VR	300x3	
ECL696	94/Sep/07	UH88	00:40:01	04:19:11	R	900x3	
ECL698	94/Sep/07	UH88	00:43:40	04:42:19	R	900x3	
ECL658	94/Sep/08	UH88	23:31:35	-03:03:23	R	900x3	
ECL660	94/Sep/08	UH88	23:35:11	-02:40:16	R	900x3	
ECL676	94/Sep/08	UH88	00:03:53	00:26:00	R	900x3	

jects using the Hubble Space Telescope. If correct, this detection would imply a magnitude-frequency slope in the range $25 \leq m_R \leq 28$ that is much steeper than $q = 3$. One troubling feature of the Cochran *et al.* measurement is that the reported detections lie within 0.2 mag of the limiting magnitude in their data. We feel that this result must be independently confirmed before it can be considered secure. It is included in Fig. 3 for completeness.

4. DISCUSSION

4.1 The Plutinos

Since 1992, it has become increasingly obvious that many trans-Neptunians are in or close to mean-motion resonances with Neptune (Marsden 1994; Paper 1). These are the objects we have called "Plutinos" to mark the dynamical kinship with Pluto. Several theories have been developed to account

TABLE 3. Observations from the Cerro-Tololo InterAmerican Observatory 1.5 m Telescope.

Field	UT Date	Tel	RA(2000)	Dec(2000)	Filter	Integration	Detected Objects
ECL597	94/May/11	CTIO	13:16:41	-08:06:08	R	900x3	
ECL598	94/May/11	CTIO	13:18:31	-08:17:11	R	900x3	
ECL599	94/May/11	CTIO	13:20:22	-08:28:22	R	900x3	
ECL600	94/May/11	CTIO	13:22:12	-08:39:10	R	900x3	
ECL668	94/May/11	CTIO	15:31:40	-19:04:44	R	900x3	
ECL669	94/May/11	CTIO	15:33:38	-19:11:38	R	900x3	1994 JS (MPEC 1994.J07)
ECL670	94/May/11	CTIO	15:35:37	-19:18:26	R	900x3	
ECL671	94/May/11	CTIO	15:37:37	-19:25:10	R	900x3	
ECL672	94/May/11	CTIO	15:39:36	-19:31:49	R	900x3	
ECL601	94/May/12	CTIO	13:24:02	-08:50:06	R	900x3	
ECL602	94/May/12	CTIO	13:25:53	-09:01:01	R	900x3	
ECL603	94/May/12	CTIO	13:27:43	-09:11:53	R	900x3	
ECL604	94/May/12	CTIO	13:29:34	-09:22:42	R	900x3	
ECL605	94/May/12	CTIO	13:31:25	-09:33:30	R	900x3	
ECL673	94/May/12	CTIO	15:41:35	-19:38:24	R	900x3	
ECL674	94/May/12	CTIO	15:43:34	-19:44:52	R	900x3	
ECL675	94/May/12	CTIO	15:45:34	-19:51:16	R	900x3	
ECL676	94/May/12	CTIO	15:47:34	-19:57:34	R	900x3	
ECL606	94/May/13	CTIO	13:33:16	-09:44:14	R	900x3	
ECL607	94/May/13	CTIO	13:35:07	-09:54:56	R	900x3	
ECL608	94/May/13	CTIO	13:36:58	-10:05:36	R	900x3	
ECL609	94/May/13	CTIO	13:38:49	-10:16:14	R	900x3	1994 JV (MPEC 1994.J09)
ECL610	94/May/13	CTIO	13:40:41	-10:26:49	R	900x3	
ECL676	94/May/13	CTIO	15:47:34	-19:57:34	R	900x3	
ECL677	94/May/13	CTIO	15:49:34	-20:03:48	R	900x3	
ECL678	94/May/13	CTIO	15:51:34	-20:09:56	R	900x3	
ECL679	94/May/13	CTIO	15:53:35	-20:16:00	R	900x3	
ECL680	94/May/13	CTIO	15:55:34	-20:21:58	R	900x3	
ECL689	95/Apr/26	CTIO	12:15:34	-01:41:43	R	900x3	
ECL690	95/Apr/26	CTIO	12:17:22	-01:52:48	R	900x3	1995 HM5 (MPEC 1995.L12)
ECL691	95/Apr/26	CTIO	12:19:12	-02:04:36	R	900x3	
ECL752	95/Apr/30	CTIO	14:07:44	-12:54:57	R	900x3	
ECL753	95/Apr/30	CTIO	14:09:37	-13:04:41	R	900x3	
ECL754	95/Apr/30	CTIO	14:11:30	-13:14:35	R	900x3	
ECL755	95/Apr/30	CTIO	14:13:24	-13:24:19	R	900x3	
ECL756	95/Apr/30	CTIO	14:15:17	-13:33:58	R	900x3	

for this observation (e.g., Malhotra 1993). The effect is shown in Fig. 4 (Plate 44), where we have plotted all 32 known Kuiper Belt objects with different symbols to distinguish objects from the present MKCT survey from those of Paper 1 and other (mostly unpublished) surveys. The locations of the major mean-motion resonances (taken from Malhotra 1996, on whose Fig. 11 this diagram is based) are marked. By far the most densely populated resonance is the 3:2 ($a = 39.39$ AU). Counting Pluto, 13 of the 33 (40%) plotted objects fall within the boundaries of the 3:2 resonance, including 6 from the MKCT survey (1994 TB, 1995 GA_7, HM_5, KK_1, QY_9, and QZ_9), 2 from Paper 1 (1993 RO and RP), 2 from Williams *et al.* (1995) (1993 SB and SC) and 1994 JR_1 and 1995 YY_3. In the $a-e$ plane, Pluto (marked by $\times$ in Fig. 4) cannot be distinguished from its neighbors. For example, its eccentricity (0.25) is equal to that of 1995 QY_9 ($e = 0.25$) and surpassed by that of 1994 TB ($e = 0.31$), while its inclination ($i = 17.1°$) is less than that of 1995 QZ_9 ($i = 19.5°$). Like Pluto, 3 trans-Neptunians (1993 SB, 1994 TB, and 1995 QY_9) have perihelia ($q = 27.2$, 29.5, and 26.8 AU, respectively) inside the orbit of Neptune (30.06 AU). These similarities are the basis for our belief that Pluto is more meaningfully regarded as the largest Kuiper Belt object than as a deviant planet.

Apart from the 13 objects near the 3:2 resonance, only 1995 DA_2 is probably trapped within a mean-motion resonance (the 4:3; Fig. 4). This relative underpopulation of the resonances interior to 3:2 (namely 6:5, 5:4, 4:3, and 7:5) is unlikely to be an observational artifact. Bodies in these resonances would be (on average) closer and, for a given diameter and albedo, brighter than those in the 3:2 resonance, and therefore easier to detect. The observed ratio of populations (again, including Pluto) is $n(3:2)/n(4:3) = 13:1$. Malhotra (1995) has calculated this ratio in the context of her resonant trapping theory. In this theory, Neptune (and the other gas giants) undergo radial migration in response to angular momentum exchange with nearby planetesimals, as part of the process by which the Oort Cloud is formed. The relative populations of the various resonances depend in part on the rate of radial migration of Neptune, raising the exciting possibility that measurements of the relative populations can be used to determine both the rate of radial migration, and the

TABLE 4. Discovery circumstances and physical properties.

Name	Discovery Date [UT]	R [AU]	Δ [AU]	α [°]	m_R	H_R	D [km]	Reference
1994 JS	94/May/11	36.03	35.02	-0.2	22.4	6.8	256	MPEC 1994-J07
1994 JV	94/May/13	34.14	33.22	0.7	22.4	7.0	237	MPEC 1994-J09
1994 TA	94/Oct/02	15.01	14.02	-0.7	22.5	10.8	42	MPEC 1994-T01
1994 TB	94/Oct/02	31.26	30.32	0.6	21.5	6.5	299	MPEC 1994-T02
1994 TG	94/Oct/02	42.25	41.25	0.0	23	7.0	261	MPEC 1994-T03
1994 TH	94/Oct/03	40.94	39.94	0.0	23	6.9	245	MPEC 1994-T04
1995 DA_2	95/Feb/24	34.01	33.13	0.8	23.4	8.0	180	MPEC 1995-E05
1995 DB_2	95/Feb/24	40.57	39.69	0.6	24.	7.9	320	MPEC 1995-E06
1995 DC_2	95/Feb/24	45.21	44.22	0.0	23.4	6.9	378	MPEC 1995-E07
1995 DW_2	95/Feb/27	18.89	18.00	-1.3	21.2	8.4	127	MPEC 1995-E13
1995 GA_7	95/Apr/03	37.87	36.87	-0.1	23	7.2	213	MPEC 1995-G13
1995 GJ	95/Apr/03	39.01	38.18	0.8	22.5	6.5	299	MPEC 1995-G07
1995 HM_5	95/Apr/26	32.53	31.66	0.9	23.1	7.9	158	MPEC 1995-K02
1995 KJ_1	95/May/30	43.47	42.52	0.5	22.5	6.1	365	MPEC 1995-L03
1995 KK_1	95/May/30	32.78	31.82	0.6	23.0	7.8	165	MPEC 1995-L04
1995 QY_9	95/Aug/31	29.93	28.92	-0.1	22.4	7.6	209	MPEC 1995-W01
1995 QZ_9	95/Aug/29	34.65	33.82	-1.0	22.5	7.0	238	MPEC 1995-W11

TABLE 6. Summary of sky-plane surface densities.

Trans-Neptunian Objects				
m_R	Area [deg^2]	N	Σ_{TN} [1] [# deg^{-2}]	Source
Photographic Surveys				
16.8	1530	1	6.5×10^{-4}	Tombaugh (1961)
19.5	6400	0	$<8.6 \times 10^{-4}$	Kowal (1989)
20.0	297	0	$<1.9 \times 10^{-2}$	Luu and Jewitt (1988)
CCD Surveys				
22.0§	4.9	0	≤ 1.1	Levison and Duncan (1990)
23.2	8.3	12	$1.4\ (^{+0.6}_{-0.6})$	This work (MKCT)
23.2	1.2	2	$1.6\ (^{+1.6}_{-1.4})$	Paper 1
23.2	9.5	14	$1.5\ (^{+0.5}_{-0.5})$	MKCT + Paper 1
23.5	0.7	2	$2.9\ (^{+2.9}_{-2.4})$	Irwin *et al.* (1995)
24.2	3.9	15	$3.8\ (^{+0.9}_{-1.0})$	This work (MKCT)
24.2	1.2	5	$4.2\ (^{+2.5}_{-2.5})$	Paper 1
24.2	5.1	17	$3.9\ (^{+1.1}_{-1.1})$	MKCT + Paper 1
24.8	1.2	7	$5.8\ (^{+3.3}_{-2.9})$	Paper 1
28.1§	10^{-3}	29?	2.5×10^4?	Cochran *et al.* (1995)

§ Calculated from limiting $m_V = 22.5$, using V-R = 0.5 (Luu and Jewitt 1996).
[1] Upper limits are 99.9% (approximately 3σ) confidence limits.

timescale for the ejection of the Oort Cloud comets. Better statistics are needed before we can make a definitive statement, but it is interesting that the measured ratio $n(3:2)/n(4:3) = 13:1$ is compatible with calculations for migration timescales $\approx 4 \times 10^6$ yr.

There are two differences between Fig. 4 and the results of the calculations by Malhotra (1995). First, the 2:1 resonance appears empty (only 1995 WY_2 falls near it), whereas in the numerical models it is not. Second, we observe a cluster of objects near $a \approx 43$ AU, $e \approx 0.0-0.1$ that is not present in the numerical results. The origin of these differences is presently not understood, and both appear deserving of additional observational attention.

TABLE 5. Orbital elements.[1]

Name	a	e	i	M	Peri	Node	Epoch
1994 JS	42.88	0.24	14.0	324.2	238.9	56.3	1995/10/10
1994 JV	35.25	0.0	18.1	0.0	180.0	28.1	1994/05/08
1994 TA	16.82	0.31	5.4	60.5	154.2	137.7	1996/04/27
1994 TB	39.32	0.31	12.1	326.4	97.7	317.3	1995/10/10
1994 TG	42.25	0.0	6.8	0.0	353.0	15.5	1994/09/25
1994 TH	40.94	0.0	16.1	0.0	356.6	12.1	1994/09/25
1995 DA_2	36.30	0.09	6.6	42.7	312.0	127.5	1996/04/27
1995 DB_2	46.28	0.13	4.1	5.5	354.7	128.6	1996/04/27
1995 DC_2	43.96	0.09	2.3	254.6	115.1	154.2	1996/04/27
1995 DW_2	25.04	0.25	4.1	3.7	4.7	178.2	1996/04/27
1995 GA_7	39.46	0.12	3.5	63.9	100.2	21.0	1995/03/24
1995 GJ	42.91	0.09	22.9	360.0	180.3	338.9	1995/03/24
1995 HM_5	39.53	0.18	4.6	3.4	354.8	186.7	1995/05/03
1995 KJ_1	43.47	0.0	2.7	0.0	180.6	47.8	1995/06/12
1995 KK_1	39.48	0.19	9.3	21.7	328.4	228.1	1995/05/23
1995 QY_9	39.41	0.25	4.8	347.5	19.7	342.1	1995/10/10
1995 QZ_9	39.43	0.12	19.5	0.09	181.9	188.0	1995/09/20

Notes
[1] Compiled from work by Brian Marsden, Smithsonian Centre for Astrophysics.

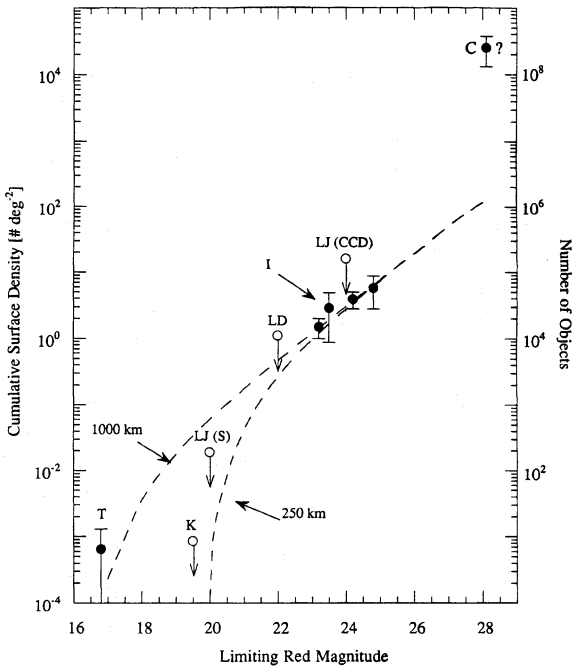

FIG. 3. Sky-plane surface densities of the Kuiper Belt, from Table 6. Filled circles with error bars denote detections, while empty circles with downward pointing arrows mark upper limits. Key: T=Tombaugh (1961), K=Kowal (1989), LJ(S) and LJ(CCD) are the Schmidt and CCD surveys of Luu & Jewitt (1988), LD=Levison & Duncan (1990), I=Irwin *et al.* (1995), and C=Cochran *et al.* (1995). The two dashed curves show the expected surface densities for power law models in which the maximum object diameter is 1000 and 250 km, as marked. The right hand axis shows the total number of objects brighter than m_R assuming ecliptic area $= 10^4$ deg^2.

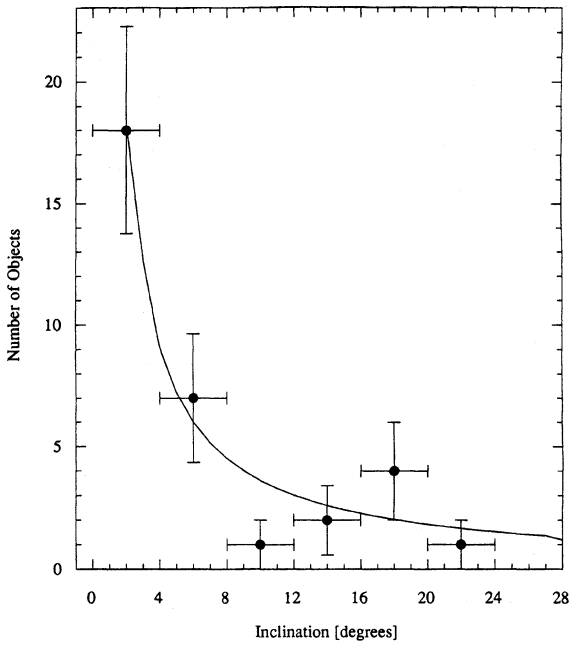

FIG. 5. Inclination distribution of the Kuiper Belt objects, binned to 4°. Error bars on the data are equal to $N^{1/2}$, where N is the number of objects per bin. The solid line shows a model fit to the data in which the inclination distribution is $N(i)$=constant for $0 \leqslant i \leqslant 30°$.

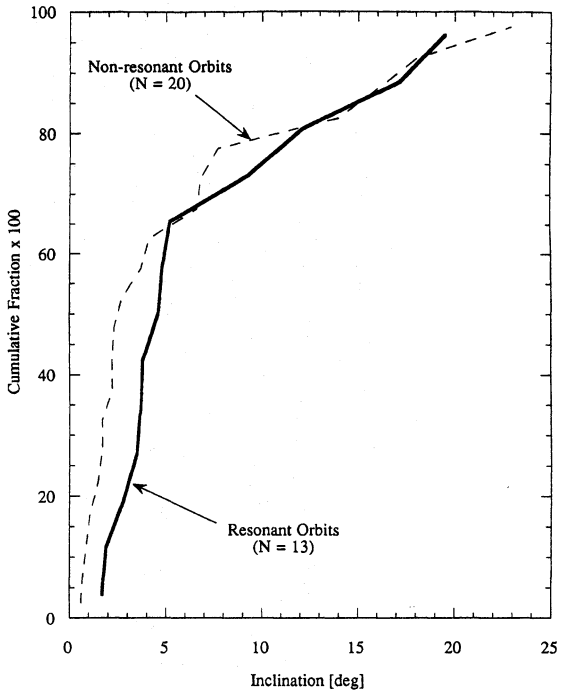

FIG. 6. The number of objects having orbital inclination $\geqslant i$ is plotted as a function of i. The dashed and solid curves show objects having non-resonant and resonant (mostly 3:2) orbits, respectively.

4.2 Inclination Distribution

The inclination distribution of the trans-Neptunians is important because it controls the velocity dispersion among these objects and hence determines whether the collisional regime is erosive or agglomerative. In addition, models of the transfer of short-period comets from the Kuiper Belt make the testable prediction that the inclination distributions of Belt objects and comets should be similar (Duncan *et al.* 1988). Fortunately, inclination is the most easily determined of the orbital parameters: it is normally measured to better than $\pm 0.5°$ in just a few nights of observation, whereas the eccentricity and semimajor axis may take months to converge.

We plot the inclination distribution of all known Kuiper Belt objects in Fig. 5. In Fig. 6 we show the cumulative inclination distributions computed separately for 13 objects (including Pluto) in the 3:2 resonance and for all other objects. The FWHM of Gaussian functions fitted to the data by least-squares, and the median inclination, i_m, are summarized in Table 7. These quantities are computed separately for all Kuiper Belt objects considered together, for the 13 objects near the 3:2 mean-motion resonance, and for the 20 objects not near the 3:2 resonance. The apparent angular width of the Kuiper Belt is 10° (FWHM). Malhotra's (1995) resonance capture simulations predict that the median inclination of objects in mean-motion resonances should be higher than those of non-resonant bodies. Table 7 hints at a difference in the expected sense but, together with Fig. 6, shows that the FWHM of the resonant objects ($13.0° \pm 3.4°$) and nonresonant objects ($8.2° \pm 1.4°$) are formally consistent.

TABLE 7. Apparent inclination distributions.

Object Subset[1]	N[2]	*FWHM* [deg][3]	i_m [deg][4]
All[A]	33	10.2 ± 1.2	3.7
3:2 Resonance[B]	13	13.0 ± 3.4	4.6
Non-resonant[C]	20	8.2 ± 1.4	2.4
Comets[D]	158	28 ± 3	10

Notes

[1] = Dynamical subset of objects; [2] = Number of objects in sample; [3] = Full Width at Half Maximum (in degrees) of a Gaussian function least-squares fitted to the inclination histogram at 2° binning resolution. The 1σ uncertainty is quoted; [4] = the median inclination (in degrees).

[A] = All known objects including Pluto; [B] = All objects in the 3:2 mean motion resonance with Neptune, including Pluto; [C] = All other Kuiper Belt Objects; [D] = Comets from Marsden (1983).

The inclination distribution of the short-period comets (Marsden 1983) is included in Table 7. The apparent FWHM $\approx 28°$ of the comets is substantially broader than that of the Kuiper Belt. Whether or not this difference is physically significant depends on the potentially large but poorly characterized effects of observational selection (in both the cometary and Kuiper Belt data sets). Accordingly, we now consider these effects in the Kuiper Belt sample.

The apparent and true inclination distributions of Kuiper Belt objects differ as a result of observational selection. Objects of high inclination spend a smaller fraction of each orbit near the ecliptic than do objects of low inclination, and are therefore less likely to be detected in ecliptic surveys such as the MKCT. For pencil-beam surveys, the probability that an object of inclination i (rad) will fall in a square field of view of side h (rad) is (Paper 1)

$$P(h,i)=\left(\frac{2}{\pi}\right)\left(\frac{h}{2\pi}\right)\sin^{-1}\left(\frac{h}{2i}\right), \quad (3)$$

which varies as $P(h,i)\propto h^2/i$ for $h/(2i)\ll 1$. We computed models of the apparent inclination distribution, $A(i)$, using $A(i)=N(i)P(h,i)$, where $N(i)$ is the intrinsic inclination distribution, and compared them with the observed distribution (Fig. 5). In view of the mix of resonant and nonresonant orbits prevailing in the inner belt, there is no physical reason why $N(i)$ should follow a simple analytic form. Nevertheless, we found it possible to represent the data of Fig. 5 using a variety of simple analytic functions. A box function, $N(i)$ = constant ($0\leqslant i\leqslant i_{max}$) and $N(i)=0$, otherwise, matched the data well provided $i_{max}\geqslant 25°$ (Fig. 5). Gaussian distributions with FWHM $\geqslant 30°$ also fit well. The main result is that the apparent distribution ($\approx 10°$ FWHM) is artificially narrow as a result of the bias against high inclination objects, as embodied in Eq. (3). The intrinsic distribution is broad ($\geqslant 30°$ FWHM) and the Kuiper Belt occupies a surprisingly thick swath of sky. A large intrinsic width also reduces the difference between the Kuiper Belt and short-period comet inclination distributions (Table 7). This result is tempered, however, by the fact that the comet inclination distribution is also influenced by observational selection.

The original inclinations of the Kuiper Belt objects must have been small in order for accretion to proceed (Bailey 1994). The perpendicular component of the orbital velocity is $V\approx V_K \sin i$, where i is the inclination and, at 40 AU, the Keplerian velocity is $V_K=5$ km s^{-1}. With $i=25°$, for example, $V=2$ km s^{-1} and the collisions would be erosive. Presumably, the inclinations now measured have been pumped by gravitational interactions with the planets since the time of formation.

Based on the available data and the bias model, we represent the Kuiper Belt as a swath 360° around by 30° tall, for a total sky area of 10^4 deg^2. This is twice the area assumed in Paper 1, and may still be an underestimate in view of the preceding discussion. Accordingly, we revise our estimate of the number of Kuiper Belt objects with diameters $2a\geqslant 100$ km in the $30\leqslant R\leqslant 50$ AU heliocentric distance range from $N=3.5\times 10^4$ (Paper 1) to $N=7\times 10^4$. Given that ~40% of the trans-Neptunians are in or near the 3:2 resonance with Neptune (Sec. *4.1*), we estimate the total Plutino population at $N\approx 3\times 10^4$ (diameters $\geqslant 100$ km). These crude estimates could easily be wrong by factors of several. However, the basic result that the 30–50 AU region is heavily populated and that it incorporates tens of thousands of Plutinos, is an inescapable conclusion of the ecliptic survey.

The total mass of a $q=3$ size distribution of spherical objects (cf. Sec. 3) is given by

$$M=\frac{8}{3}\pi\rho N a_-^2(a_+-a_-), \quad (4)$$

where ρ (kg m^{-3}) is the bulk density of the objects, the radii lie in the range $a_-\leqslant a\leqslant a_+$ with $a_+\gg a_-$, and N is the number of objects in this range. For example, with $\rho=1000$ kg m^{-3}, $N=7\times 10^4$, $a_-=50$ km, and $a_+=250$ km (corresponding to the lower curve in Fig. 3), we obtain $M=3.7\times 10^{23}$ kg (0.06 $\mathscr{M}_{Earth}$, where 1 $\mathscr{M}_{Earth}=6\times 10^{24}$ kg). Increasing a_+ to 1000 km (upper curve in Fig. 3) would give $M=1.5\times 10^{24}$ kg (0.25 $\mathscr{M}_{Earth}$). These mass estimates depend on the unknown upper limit to the size distribution and are correspondingly uncertain. Nevertheless, it is clear that the inner Kuiper Belt holds a substantial mass in objects larger than 100 km diameter. Even the higher of the two mass estimates is compatible with the ~1 $\mathscr{M}_{Earth}$ upper limit set by the absence of precession of the orbit of comet P/Halley (Hamid *et al.* 1968; Hogg *et al.* 1991).

In this section we have considered inclinations measured relative to the ecliptic plane. The Kuiper Belt objects are more likely to respect the Laplace plane, defined by the gravitational potentials of the planets (especially the massive gas giant planets). Accordingly, we recomputed the inclinations with respect to the Laplace plane (taken to be inclined to the ecliptic by 1.6° and with ascending node at 107°: Liou & Dermott 1994). Within the binning uncertainties, we found no dependence of the inclination distribution on the adopted reference plane.

4.3 The Number of Centaurs

The newly discovered Centaurs are the Uranus-crosser 1994 TA ($q=11.68$ AU, $Q=21.96$ AU) and 1995 DW$_2$ ($q=18.86$, $Q=31.21$ AU), which crosses the orbits of both Uranus and Neptune. 1994 TA approaches the orbit of Saturn sufficiently closely that we expect its motion to be heavily influenced by that planet as well as by Uranus. As with the more familiar 2060 Chiron and 5145 Pholus at smaller distances, these objects are presumed to be dynamically unstable. The diameters of 1994 TA and 1995 DW$_2$ are ≈ 40 and ≈ 130 km, respectively (Table 4), when computed in the same way as for the trans-Neptunians.

The detection of two Centaurs in the tiny fraction of the ecliptic so far surveyed immediately shows that the Centaur population must be very large. The sky-plane surface density is

$$\Sigma_C(m_R\leqslant 24.2)=0.5\pm 0.4 \text{ deg}^{-2}. \quad (5)$$

If, like the Kuiper Belt objects, the Centaurs occupy a projected area of order 10^4 deg^2, the number of such objects brighter than $m_R=24.2$ must be of order 5000 (with an uncertainty of a factor of several, due to the limited statistics and to uncertainty in the adopted sky area). Evidently, the six known Centaurs represent the tip of a very large iceberg.

The conversion of the measured sky-plane Centaur surface density [Eq. (5)] to the physically more interesting number density (i.e., number of Centaurs per AU^3) requires the adoption of a model for the radial distribution of Centaurs. In the absence of such a model, we make a simple calculation which has the advantage of being independent of any theory and therefore robust. At $R=30$ AU, $\Delta=R-1=29$ AU, the limiting magnitude $m_R=24.2$ corresponds to absolute magnitude $H_R=9.5$ (diameter≈ 75 km). Centaurs with $H_R\leqslant 9.5$ would be detectable by the MKCT survey at any distance in the range $10\leqslant R\leqslant 30$ AU. Centaur 1995 DW$_2$ has $H_R=8.4$ (Table 4) and so falls into this group, while 1994 TA ($H_R=10.8$) is a smaller object that was detected because of its smaller distance ($R=15$ AU at the time of discovery). Therefore, in the distance range $10\leqslant R\leqslant 30$ AU, we detected

one Centaur with $H_R \leq 9.5$ in 3.9 deg^2. In 10^4 deg^2, we obtain the total population of Centaurs $N(H_R \leq 9.5) \approx 2600$ (for comparison, the number of main-belt asteroids with $H_R \leq 9.5$ is approximately 350). From Eq. (4) with $N = 2600$, $\rho = 10^3$ kg m^{-3}, $a_+ = 250$ km, $a_- = 75$ km ($H_R = 9.5$), we find a total Centaur mass of order 2×10^{22} kg (3.5×10^{-3} $\mathcal{M}_{\rm Earth}$). The mean dynamical lifetime for transfer from Neptune-crossing to Jupiter-crossing orbits is $t_c \approx 10^7$ yr (see below). Hence, the Centaur population must have been replenished $\approx$450 times since the formation of the solar system, and the total mass cycled through the Centaurs is of order 1×10^{25} kg (1.5 $\mathcal{M}_{\rm Earth}$). This is large compared to the mass of the present-day Kuiper Belt in the 30–50 AU region (0.06–0.25 $\mathcal{M}_{\rm Earth}$: Sec. *4.2*), and suggests that the inner portions of the Kuiper Belt have been heavily eroded since formation (cf. Holman & Wisdom 1993; Duncan *et al.* 1995). These are crude calculations of the mass but they are also conservative. For example, we neglected Centaurs with $a < 75$ km because they are too faint to be detected throughout the $10 \leq R \leq 30$ AU range, and we neglected rare Charon-like objects with $a > 250$ km.

Independent observational estimates of the Centaur population are lacking in the published literature. The Space-Watch project is potentially of great value in this regard. It has discovered 3 Centaurs (5145 Pholus, 1993 HA_2, and 1995 GO; Scotti 1994), but the sky area surveyed and parameters of the survey have not yet been published. Kowal (1989) discovered the first Centaur, 2060 Chiron, in a survey of 6000 deg^2, for a surface density $\Sigma_C(m_R \leq 19.5) \approx 2 \times 10^{-4}$ deg^{-2}. However, the long integration times forced by his use of photographic detectors result in potentially severe trailing loss for objects at Centaur distances. For example, at $R = 30$ AU, the opposition angular rate is $d\theta/dt = 3$ arcsec/hr, and for a 1 hr integration under seeing of 1 arcsec (FWHM), we have $\Psi = 3$ (Sec. 2), and $\Delta m_R = 1.2$ mag. At $R = 10$ AU, the corresponding quantities rise to $d\theta/dt = 12.5$ arcsec/hr, $\Psi = 12.5$, and $\Delta m_R = 2.7$ mag. This progressive trailing loss went undiscussed in Kowal's paper. Accordingly, we believe that his measurement provides only a lower limit to the surface density of Centaurs with $m_R \leq 19.5$. The Kowal and MKCT constraints are plotted in Fig. 7.

The ratio of the number of Centaurs to the number of Kuiper Belt objects should be of the same order as the ratio of the dynamical lifetimes of the Centaurs to those of Kuiper Belt objects. Using an argument of this kind, and scaling from the number of trans-Neptunian objects, Irwin *et al.* (1995) estimated a Centaur surface density much less than that in Eq. (5), namely, $\Sigma_C(m_R \leq 24.2) \approx 10^{-2}$ deg^{-2}. If Σ_C were this small, we should expect to find zero Centaurs in the limited area of the MKCT CCD survey. Specifically, in a Poisson distribution with mean $\Sigma_C = 10^{-2}$ deg^{-2}, the probability of detecting one object in 3.9 deg^2 is 4×10^{-2}, while the probability of finding two objects is only 8×10^{-4}. The empirical sky-plane density $\Sigma_C(m_R \leq 24.2) \approx 0.5$ deg^{-2} is about 50 times larger than the Irwin *et al.* estimate. This is shown graphically in Fig. 7, adapted from Irwin *et al.*'s Fig. 6. We emphasize that Centaurs inside 10 AU will be underrepresented in our data as a result of the trailing loss, and that $\Sigma_C(m_R \leq 24.2) \approx 0.5$ deg^{-2} is therefore to be considered as a lower limit.

The excess number of Centaurs is something of a puzzle, to which we consider several possible solutions.

First, the possibility that the dynamical lifetimes of the Centaurs might be underestimated by a factor $\sim$50 seems unlikely. An uncertainty of a factor 3–10 is quoted by Irwin *et al.* (1995), who take the lifetimes of Uranus and Neptune-crossers to be of order 10^7 yr. Numerical integrations of general orbits in the gas giant region by Gladman & Duncan (1990) and Holman & Wisdom (1993) yield consistently short dynamical lifetimes, as do integrations specific to 2060 Chiron (10^5–10^6 yr; Hahn & Bailey 1990) and 5145 Pholus (10^5–10^6 yr, Asher & Steel 1993).

Second, in-bound Kuiper Belt objects might fragment, spawning many "daughter" objects for each "parent" (Hahn & Bailey 1990; Pittich & Rickman 1994). The number of Centaurs would then be larger than the number of objects transferred to the gas giant region from the Kuiper Belt by the ratio of the number of daughters to the number of parents. The nuclei of comets (which are presumably small ex-Centaurs) are known to split, at a rate estimated at 10^{-2} per year per nucleus (Chen & Jewitt 1994). Splitting of comets may be due to (1) rotational bursting, (2) pressure forces exerted by embedded supervolatiles, or (3) tidal disruption upon passage within the Roche spheres of the Sun or gas giant planets. The known Centaurs are too massive for rotational spin-up to occur within their limited dynamical lifetimes. Splitting due to gas pressure is also unlikely since the speed of sound in sublimated gas and the gravitational escape speed from a 100-km-diameter ice body are both on the order of 100 m s^{-1} (i.e., the gas carries too little momentum to cause a split). Therefore, processes (1) and (2) can be ignored in the present context. However, tidal disruption by the giant planets might be a significant source of fragments with which to amplify the Centaur population. In the present context, tidal disruptions of 100 km sized Centaurs would need to occur on 10^6–10^7 yr intervals (the dynamical lifetimes of these objects), if a steady state is to be maintained.

We possess good evidence that small comets disrupt when passing through the Roche sphere of Jupiter. Comet P/Brooks 2 fragmented in 1887 when passing ~ 2 R_J ($R_J = 7 \times 10^7$ m) from the center of Jupiter, while P/Shoemaker-Levy 9 was likewise disrupted at 1.3 R_J in 1992. Together, these examples suggest that the interval between tidal disruptions of comets by Jupiter is $\tau \approx 10^2$ yr. Comets P/Brooks 2 and P/Shoemaker-Levy 9 were probably only $\approx$2–5 km in size. Tidal disruptions of 100 km scale bodies would be comparatively rare but not fundamentally different in nature from those witnessed in the smaller comets. If the differential size distribution varies as $N(a)da \propto a^{-3}da$ (Shoemaker & Wolfe 1982), the timescale for disruption of 100 km scale Centaurs would be $\approx [N(100)/(N(2 \text{ to } 5)]^{-3}\tau \approx 10^6$–$10^7$ yr. In another context, Dones (1991) estimated that 10–100 Chiron sized objects would pass within Saturn's Roche sphere per 4.5 Gyr, corresponding to a mean interval in the range 4.5×10^7–4.5×10^8 yr. When augmented to account for disruptions caused by the other gas giants, especially Jupiter, his estimate would inde-

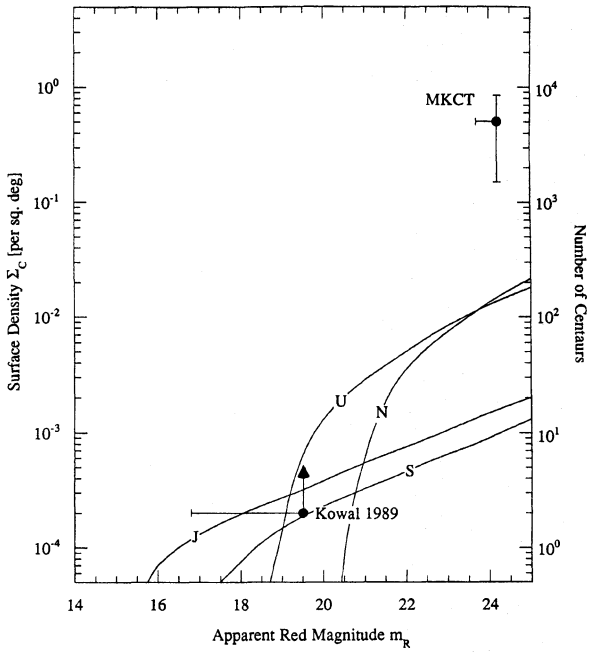

FIG. 7. Comparison of the measured sky-plane Centaur densities with the models of Irwin *et al.* (1995). The labeled curves denoted the predicted surface density of Centaurs crossing the orbits of the planets J=Jupiter, S=Saturn, U=Uranus, N=Neptune (e.g., the Neptune curve shows all Centaurs which cross the orbit of Neptune). The datum marks the Centaur surface density deduced from MKCT data. The horizontal error bars show the effect of the maximum trailing loss expected in the two surveys for Centaurs at 10 AU (see Fig. 2). The right-hand axis shows the number of Centaurs brighter than m_R assuming ecliptic area=10^4 deg^2.

pendently suggest that Centaur breakup may occur on timescales comparable to the mean dynamical lifetime. Lastly, a "particle in a box" calculation based on our estimate of 2600 large Centaurs in a disk-like volume 10 AU thick and extending from 10 to 30 AU gives a mean time between planetary encounters $t_e \approx 10^4$ yr (the encounter radius was assumed to be 2 R_J, the velocity dispersion=5 km s^{-1} and we included gravitational focusing). The number of fragments produced is $n_f \approx (t_c/t_e)f$, where f=number of fragments produced per Centaur disruption. Taking $t_c \approx 10^6 - 10^7$ yr, $f \approx 10$ (as suggested by the disruptions of P/Brooks 2 and P/Shoemaker-Levy 9), we find $n_f \approx 10^3 - 10^4$, which is of the same order as the Centaur population. Uncertainties in our knowledge of the Centaur population, and in the physics of breakup (e.g., how many daughters are produced per parent and what is their size distribution?) undermine any attempt at a more detailed calculation. At this stage we wish only to note the intriguing possibility that tidal disruption might measurably amplify the Centaur population. The expectation that the Centaur size distribution would be biassed towards smaller sizes compared to the Kuiper Belt size distribution cannot be observationally tested at the present time, since we lack albedo/diameter determinations for a substantial number of objects.

A third possible explanation for the excess density of the Centaurs is that their brightnesses might not accurately reflect their sizes, either because the assumed albedos are too low, or because the cross-sections are too high. For example, Kuiper Belt objects deflected into Centaur orbits might develop high albedo ice mantles, as a result of outgassing by embedded volatiles. The higher albedos would inflate Σ_C by raising small and otherwise undetectable objects above the threshold for detection. However, available albedo data for the Centaurs provide less than compelling support for this hypothesis. Specifically, the albedo of Centaur 5145 Pholus is only 0.04±0.01 (Davies *et al.* 1993). The albedo of 2060 Chiron is slightly higher, 0.14 $(^{+0.06}_{-0.03})$ (Campins *et al.* 1994), but may be elevated by near-nucleus dust coma contamination. At the time of writing, no Kuiper Belt albedos have been measured. Near-nucleus dust might artificially increase the scattering cross-sections of the Centaurs, leading to overestimation of their diameters. Indeed, activity in Centaur 2060 Chiron was first detected from anomalous brightening at $R \approx 10-20$ AU. Carbon monoxide and other abundant molecules would be volatile at even larger distances. Clearly, this third hypothesis could be observationally tested using measurements of the albedos, and by searching for photometric evidence of on-going mass loss in other Centaurs.

Presumably, it is also possible that two or more of the above processes act together to maintain the magnitude-limited Centaur population at an elevated level. For example, the dynamical lifetimes may be several times larger than assumed by Irwin *et al.*, and the number of Centaurs may be further enhanced by tidal splitting. Alternatively, the Centaurs may have an unconsidered source in addition to the Kuiper Belt. In short, the cause of the apparent excess in the density of Centaurs is not known, and our current understanding of these objects needs to be improved before an explanation is reached.

4.4 The Future

Several of the issues raised in this report point to the need for larger samples of Kuiper Belt and Centaur objects. In particular, accurate determination of the relative populations in the trans-Neptunian mean motion resonances (Sec. *4.1*) and of the intrinsic inclination distribution (Sec. *4.2*) will demand a larger observational sample. Using the Tektronix 2048 chips, we might reasonably expect hard work to yield a sample of 100 Kuiper Belt objects by the end of the 20th century. More rapid progress will demand the use of larger CCDs and automated detection techniques. The University of Hawaii 8192×8192 CCD camera is of great promise in this regard, and we are now exploring methods for handling the prodigious quantities of data produced by this instrument when used in survey mode.

5. SUMMARY

The outer solar system is a richly populated region whose constituents have so far escaped detailed investigation as a result of their vast heliocentric distances and resulting faintness. In this paper, we present new observational constraints on both the Kuiper Belt objects and Centaurs.

(1) At MKO we surveyed 3.9 deg^2 to limiting red magnitude $m_R = 24.2$. In this area, we detected 12 Kuiper Belt objects and 2 Centaurs. At CTIO we surveyed 4.4 deg^2 to limiting red magnitude $m_R = 23.2$, and detected 3 new Kuiper Belt objects.

(2) The sky-plane surface density of Kuiper Belt objects is $\Sigma_{TN} \approx 1.5$ deg^{-2} to limiting red magnitude $m_R = 23.2$ and $\Sigma_{TN} \approx 3.9$ deg^{-2} to $m_R = 24.2$. These values are in concordance with those previously measured (Paper 1), and can now be considered well determined quantities.

(3) The apparent width of the Kuiper Belt is $\approx 10°$ FWHM. After correcting for observational bias in favor of low inclination objects, we find that the intrinsic width of the belt must be at least 30° in order to match the data. The increased width of the belt leads us to revise our (Paper 1) estimate of its population. We estimate that at least 7×10^4 objects with diameters $\geqslant 100$ km exist in the 30–50 AU heliocentric distance range.

(4) Twelve of the 32 trans-Neptunians, in addition to Pluto, lie in or near the 3:2 mean-motion resonance with Neptune. The total number of such objects that are larger than 100 km in diameter is estimated to be of order 3×10^4. This result establishes Pluto as the largest of a hitherto unknown family of dynamically similar bodies, and effectively changes its status from that of "smallest planet" to "largest known Kuiper Belt object."

(5) The sky-plane surface density of Centaurs is $\Sigma_C(m_R \leqslant 24.2) \approx 0.5$ deg^{-2}. This is 50 times the surface density estimated by Irwin *et al.* (1995) on the basis of the estimated dynamical lifetimes. The total number of Centaurs having apparent magnitude $m_R \leqslant 24.2$ is ≈ 5000. The total number with absolute magnitude $H_R \leqslant 9.5$ (corresponding to radii $\geqslant 75$ km if albedo ≈ 0.04) is ≈ 2600 (in the distance range $10 \leqslant R \leqslant 30$ AU). The Centaur population might be amplified by tidal fragmentation by the gas giant planets, and by underestimation of their albedos or overestimation of their cross sections due to unresolved, near-nucleus dust. Alternatively, the Centaurs might have a source in addition to the Kuiper Belt.

We thank operators Dave Woodworth, Morning Roberts, and John Dvorak at the UH telescope, and Luis Gonzales and Mauricio Fernandez at CTIO. We greatly appreciate funding of this work by NASA's Origins of Solar Systems Program. Direct support of the UH telescope by NASA's Planetary Astronomy Program was instrumental in securing dark time for this project.

REFERENCES

Asher, D. J., & Steel, D. I. 1993, MNRAS, 263, 179
Bailey, M. E. 1994, in Asteroids, Comets, Meteors 1993, edited by A. Milani *et al.* (Kluwer, Dordrecht), pp. 443–459
Bowell, E., Hapke, B., Domingue, D., Lumme, K., Peltoniemi, J., & Harris, A. 1989, in Asteroids II, edited by R. Binzel, T. Gehrels, and M. Matthews (University of Arizona Press, Tucson), pp. 524–556
Campins, H., Telesco, C., Osip, D., Rieke, G., Rieke, M., & Schulz, B. 1994, AJ, 108, 2318
Chen, J., & Jewitt, D. C. 1994, Icarus, 108, 265
Cochran, A. L., Levison, H. F., Stern, S. A., & Duncan, M. J. 1995, AJ, 455, 342
Davies, J., Spencer, J., Sykes, M., Tholen, D., & Green, S. 1993, IAU Circ. No., 5698
Dones, L. 1991, Icarus, 92, 194
Duncan, M., Quinn, T., & Tremaine, S. 1988, ApJ, 328, L69
Duncan, M., Levison, H. F., & Budd, S. M. 1995, AJ, 110, 3073
Edgeworth, K. E. 1949, MNRAS, 109, 600
Fernandez, J. A. 1980, MNRAS, 192, 481
Gladman, B., & Duncan, M. 1990, AJ, 100, 1680
Hahn, G., & Bailey, M. E. 1990, Nature, 348, 132
Hamid, S. E., Marsden, B., & Whipple, F. 1968, AJ, 73, 727
Hogg, D. W., Quinlan, G. D., & Tremaine, S. 1991, AJ, 101, 2274
Holman, M., & Wisdom, J. 1993, AJ, 105, 1987
Irwin, M., Tremaine, S., & Zytkow, A. N. 1995, AJ, 110, 3082
Jewitt, D. 1996, Earth, Moon, and Planets, 72, 185
Jewitt, D. C., & Luu, J. X. 1993, Nature, 362, 730
Jewitt, D. C., & Luu, J. X. 1995, AJ, 109 (Paper 1)
Kowal, C. 1989, Icarus, 77, 118
Kuiper, G. P. 1951, in Astrophysics, edited by J. A. Hynek (McGraw–Hill, New York), pp. 357–424
Landolt, A. 1992, AJ, 104, 340
Levison, H. F., & Duncan, M. J. 1990, AJ, 100, 1669
Liou, J. C., & Dermott, S. F. 1994, unpublished manuscript
Luu, J. 1994, in Asteroids, Comets, Meteors 1993, edited by A. Milani *et al.* (Kluwer, Dordrecht), pp. 31–44
Luu, J. X., & Jewitt, D. 1988, AJ, 95, 1256
Luu, J., & Jewitt, D. 1995, AJ, 111, 499
Luu, J. X., & Jewitt, D. C. 1996, AJ (in press)
Malhotra, R. 1993, Nature, 365, 819
Malhotra, R. 1995, AJ, 110, 420
Malhotra, R. 1996, AJ, 111, 504
Marsden, B. G. 1983, Catalog of Cometary Orbits (Enslow, New Jersey)
Marsden, B. G. 1989, AJ, 98, 2306
Marsden, B. G. 1994, IAUC 6076 (September 10)
Morbidelli, A., Thomas, F., & Moons, M. 1995, Icarus, 118, 322
Pittich, E. M., & Rickman, H. 1994, A&Ap, 281, 579
Scotti, J. V. 1994, in Asteroids, Comets, Meteors 1993, edited by A. Milani, M. di Martino, and A. Cellino (Kluwer, Dordrecht), p. 17
Shoemaker, E. M., & Wolfe, R. F. 1982, in Satellites of Jupiter, edited by D. Morrison (University of Arizona Press, Tucson), pp. 277–339
Tombaugh, C. W. 1961, in *Planets and Satellites*, edited by G. P. Kuiper and B. M. Middlehurst (University of Chicago Press, Chicago), pp. 12–30
Williams, I. P., O'Ceallaigh, D. P., Fitzsimmons, A., & Marsden, B. G. 1995, Icarus, 116, 180

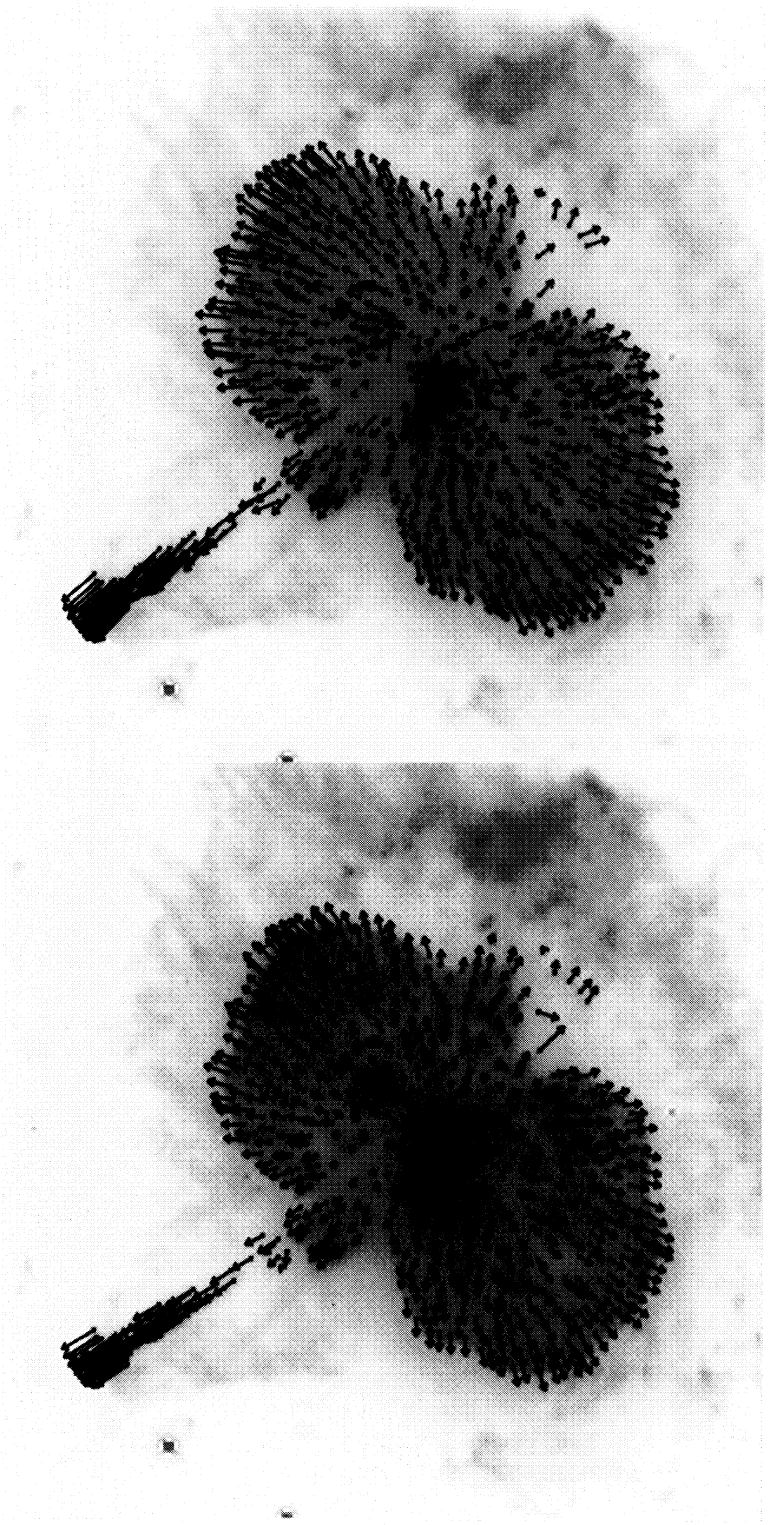

FIG. 5. The astrometric displacement vectors for the PC1:WF2 (left) and WF1:WF2 (right) comparisons. The actual magnitude of the motion is 1/5 the length of the arrows.

Currie *et al.* (see page 1122)

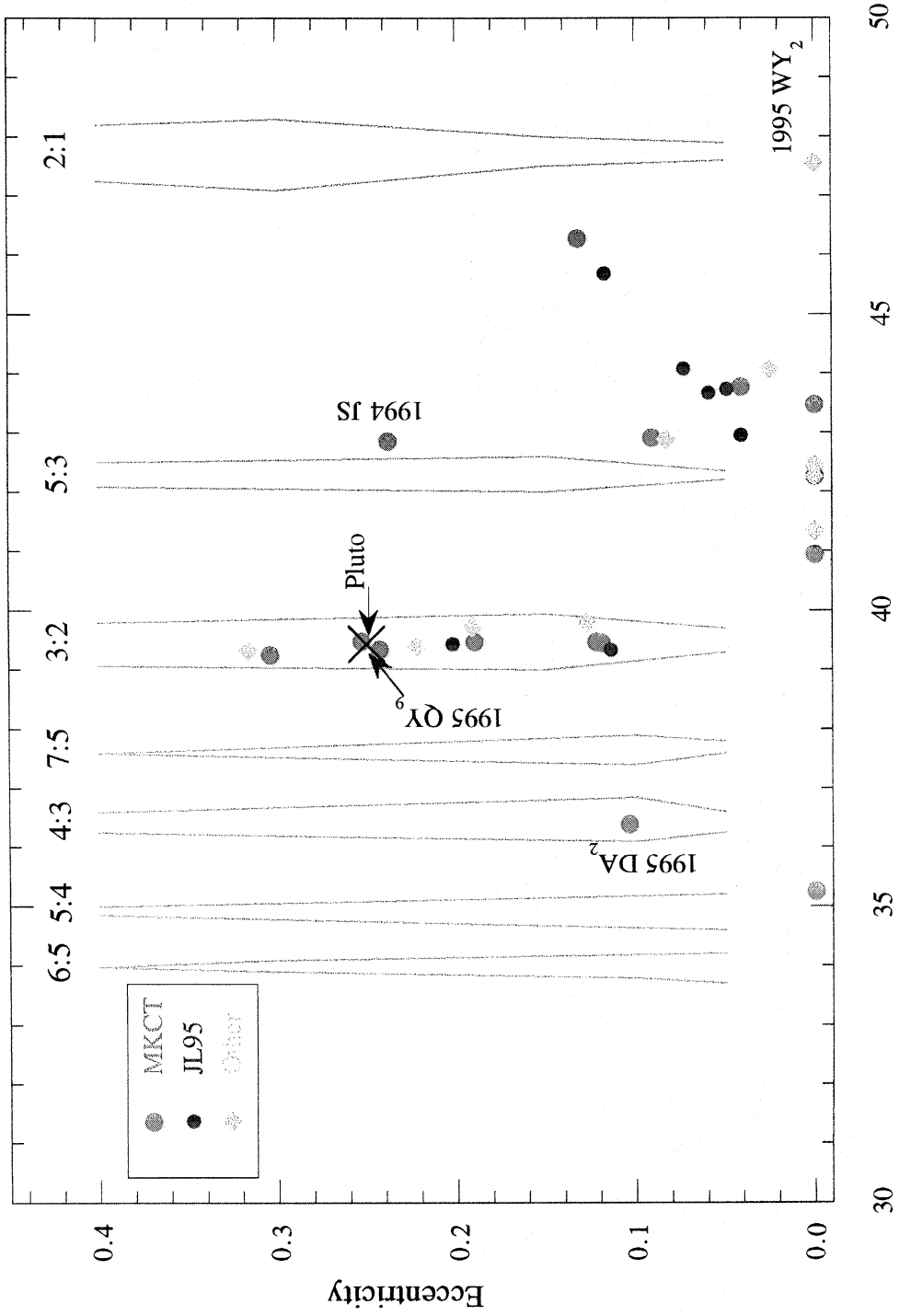

FIG. 4. Semimajor axis vs eccentricity for the known Kuiper Belt objects. The plot shows objects from the MKCT survey (red circles), the deeper survey of Paper I (blue circles) and other objects (pale blue diamonds). The location of the major mean-motion resonances (taken from Malhotra 1996, on whose Fig. 11 this diagram is based) are marked and labelled. An excess of objects in the 3:2 resonance is clearly apparent. Pluto, also in the 3:2 resonance, is marked with an X. The number of objects in this plot is less than the number of known trans-Neptunians because of overlap at the scale of the figure. Note also that 1995 QY_9 is coincident with Pluto in the $a-e$ plane.

Jewitt *et al.* (see page 1232)